submitted to Journal of Non-Crystalline Solids(2007)

# Structural instability and the metal-non-metal transition in expanded fluid metals

K. Tamura[1]*, M. Inui[2], K. Matsuda[1] and D. Ishikawa[1,3]

[1]Graduate School of Engineering, Kyoto University, Kyoto 606-8501, Japan

[2] Graduate School of Integrated Arts and Sciences, Hiroshima University, Higashi-Hiroshima 739-8521, Japan

[3]SPring-8/RIKEN, Sayo-cho, Sayo-gun, Hyogo 679-5148, Japan

Footnote

Corresponding author e-mail address: tamura@materials.mbox.media.kyoto-u.ac.jp

Abstract

X-ray diffraction, small angle X-ray scattering and inelastic X-ray scattering measurements for fluid Hg in the wide density range up to the supercritical region have been carried out using synchrotron radiation at SPring-8. We obtained the static and dynamic structure factors as a function of temperature, pressure and density. Based on the results we found that there exist medium-range fluctuations accompanying the metal-non-metal transition in fluid Hg. The scale of the fluctuations was about 10 A in space and sub-picoseconds in time. We discuss the possibility that such structural instability induces the metal-non-metal transition in expanded fluid Hg.

PACS codes: 61.10.-i, 61.25.Mv, 62.50.+p, 71.30.h+

## 1. Introduction

Metals finally transform into insulating state when they sufficiently expand. A simple band model predicts that divalent metals such as Hg transform to an insulating state with volume expansion by forming an energy gap between s and p bands. The simple band picture does not explain the transition to insulating states in monovalent metals such as alkali metals. Conduction electrons in monovalent metals at normal condition behave as nearly free electrons, which screen the positive charge of ions and occupy half of the conduction band. When the density of electrons is sufficiently reduced the screening becomes weak and conduction electrons are not free any more. The band picture of one-electron approximation becomes incorrect and the correlation between electrons is considered to be crucial for the metal-nonmetal (M-NM) transition in expanded monovalent metals.

For actual materials, a substantial and continuous volume expansion from the liquid to the rarefied vapor surrounding the liquid vapor critical point may be possible by controlling the temperature and pressure, which allows us to study the M-NM transition in fluid metals. In the expansion process the mean interatomic distance increases up to ten times larger than that at normal condition and the electronic properties change dramatically.

The evidence of the M-NM transition with volume expansion has been obtained by the measurements of the direct-current conductivity for fluid Hg [1], and fluid Rb and Cs [2]. These fluid metals have been extensively investigated so far [3] because the critical temperatures and pressures are relatively low so that the physical properties can be investigated in the laboratory. It is widely known that the M-NM transition in fluid Hg starts to occur when

the density decreases down to 9 g $cm^{-3}$ larger than the critical density (critical data of Hg [4]: $T_c$=1478 C, $p_c$=1673 bar, $\rho_c$=5.8 g $cm^{-3}$) while monovalent metals such as fluid Rb and Cs undergo the M-NM transition around the critical density.

It is interesting to study how atomic arrangements change with volume expansion. The volume expansion of fluids is essentially caused by thermal effects, in which pressure is applied to suppress the boiling. The thermal expansion in fluids is different from that of crystals. In crystals the thermal expansion originates from the anharmonic nature of the vibration of constituent atoms and the crystal symmetry does not change during the thermal expansion, that is, the coordination number remains unchanged while the interatomic distance increases. In fluids the same type of expansion possibly occurs keeping the coordination number constant and increasing the interatomic distance. In addition, another one way may be possible in fluids, in which the coordination number decreases and the interatomic distance remains constant. Recent structural investigations revealed that the latter type of expansion occurs in fluid Hg [5], Rb [6] and Cs [7]. Fluid metals expand inhomogeneously as if atoms in the random array are taken away one by one, and appear to favor this way in which configurational entropy increases. This is the gross feature of structural changes in the expansion process from liquid to vapor.

It seems that such an inhomogeneous expansion stimulates the formation of clusters or molecules in sufficiently expanded fluids. Especially when the electronic states dramatically change with the M-NM transition, electrons may assist the formation of clusters. A recent investigation on expanded fluid Rb [8], for instance, suggests that dimers are already formed in the metallic region near the critical point. It has been pointed out [9] that the existence of dimers in the metallic region of fluid Rb is helpful to understand the structural changes in the

metallization process of compressed fluid hydrogen (H); recently metallic fluid H has been obtained at high temperature and high pressure by a shock compression [10].

Thus, it is important to obtain detailed information on the structural changes of expanded fluid metals. We have been promoting a five years project on the structural investigation of expanded fluid metals such as Hg, Rb and Se using synchrotron radiation at SPring-8 and accumulated the data on static and dynamic structures as a function of temperature, pressure and density. In the present paper we review our advanced results of X-ray diffraction (XD), small angle X-ray scattering (SAXS) and inelastic X-ray scattering (IXS) measurements for fluid Hg focusing on the M-NM transition. We discuss the relationship between the structural instability in the medium range and the M-NM transition in fluid Hg.

## 2. Experimental

We performed energy-dispersive XD measurements for expanded fluid Hg using synchrotron radiation on the BL04B1 at SPring-8. The storage ring at SPring-8 was operated at 8 GeV with 100 mA during the present experiments. White X-rays were incident on the sample and the scattered X-rays were detected with a pure Ge solid state detector. The details of the experimental set-up are described elsewhere [11, 12]. SAXS measurements were carried out using synchrotron radiation on the BL04B2 at SPring-8. The details of the BL04B2 beamline are given in the literature [13]. For SAXS measurements, monochromatized X-rays of 38 KeV were incident on the sample and the scattered X-rays were detected with an imaging plate. An ionization chamber was put in front of the imaging plate before and after a SAXS measurement to measure the intensity of the transmitted X-rays for the absorption correction. The details of

the SAXS measurements are described elsewhere [14]. IXS measurements were carried out on the BL35XU beamline at SPring-8. At the present experiment, the energy resolution of about 1.7 meV (slightly degraded because the high pressure vessel used for the present experiment forced the detector away from the best position) was achieved for monochromatized X-ray of 21.75 KeV from Si (11 11 11) reflection. The resolution is an order of magnitude larger than inelastic neutron scattering experiments. However the fact that the available beam size of 0.1 x 0.1 $mm^2$ is much smaller than neutron beam is greatly proper for the measurements at extreme condition of high temperatures and high pressures. The details of the BL35XU beamline are reported in the literature [15].

The experiments at high temperature and high pressure were performed using an internally heated high-pressure vessel made of super-high-tension steel. The apparatus permits measurements to be made up to 1700 C and 2000 bar by the He-gas compression. The high-pressure vessel for XD measurements has seven Be windows for scattered X-rays, which are located at different scattering angles $2\theta$ to cover a sufficiently wide range of a modulus of scattering vector $k$ ($k=4\pi sin\theta/\lambda$, where $\lambda$ is a wave length). The vessel for the SAXS measurements has a window using a synthetic diamond with the highest quality of 3 mm in diameter with 2 mm in thickness for incident X-rays and that of 6 mm in diameter with 2.5 mm in thickness for outgoing X-rays. The construction of the high-pressure vessels for the XD and SAXS measurements are shown elsewhere [12]. We developed a vessel for IXS measurements and installed a high-pressure gas apparatus in the experimental hutch at BL35XU. The design is essentially the same as those for XD and SAXS measurements. To withstand high pressure up to 2000 bar, the vessel for IXS measurements could not be equipped with large windows. So Be

windows for incident and scattered X-rays are located at discrete scattering angles. By choosing a pair of the Be windows for incident and scattered X-rays, we can measure IXS spectra at a scattering angle. The details of the construction are described in the literature [16].

Supercritical fluid Hg must be contained in a cell made of a special material that is transparent to X-rays and resistant to chemical corrosion by hot fluid Hg. A single-crystalline sapphire cell was developed for this purpose and the details are described elsewhere [17]. The cell consists of a hot part and a sample reservoir kept around the melting temperature of the liquid sample. The liquid sample was introduced from the reservoir to the small gap between two closed-ends of sapphire cell at the hot part. The sample thickness was several ten to hundred μm. The closed-ends through which X-rays pass were made as thin as possible, with a thickness of 150 μm. The hot part was heated by a tungsten (W) heater surrounding a molybdenum (Mo) tube to keep the temperature uniform. The sapphire cell was put into the Mo tube. The sample was contained in a single-crystalline sapphire cell for XD measurements. For SAXS experiments a cell made of polycrystalline sapphire was used. No parasitic scattering was observed from the cell even at high temperature. For IXS measurements a single-crystalline sapphire cell was used because polycrystalline sapphire was found to generate background intensity larger than single-crystalline one.

## 3. Results

### 3.1 X-ray diffraction

The XD measurements were carried out for expanded fluid Hg for a wide temperature and pressure range up to 1540 C and 1949 bar along the saturated vapor-pressure curve, with

densities ranging from 13.6 to 1.9 g $cm^{-3}$. Figure 1 shows $S(k)$ for fluid Hg, the most recent results [18] from liquid to dense vapor through the M-NM transition and the critical density regions. The present results are of high quality compared with previous ones [5]. The use of a new high-pressure vessel with seven windows for scattered X-rays enabled us to make data analysis more reliable.

In a previous paper [19], we estimated the densities of fluid Hg from the measured temperature and pressure points on the phase diagram [4]. However, especially in the region near the critical densities, a small difference between the temperature of the sample at the position irradiated with X-rays and that of the position of the thermocouples would give a large deviation between the estimated density and the real one. We corrected the real density of the sample by measuring the absorption of X-rays or using the fact that the onset of the observed XD spectra is shifted to higher energy with increasing density. The details of data analysis are described in the literature [16, 18].

Figure 2 shows the pair distribution function $g(r)$ calculated from the Fourier transforms of $S(k)$, of fluid Hg shown in Fig. 1. The data for $g(r)$ at 25 C and 9.8 bar have several features; the first peak has an asymmetric shape, the first minimum is invariant in the region from 4 to 5 A, and the second peak is rather small. With increasing temperature and pressure, with decreasing density, the long-range oscillation of $g(r)$ diminishes. The broadening of the first peak gradually occurs but no change of the peak position is observed and the asymmetry of the first peak remains at temperatures and pressures up to 1495 C and 1940 bar. While the first peak is observable even in the M-NM transition region, the second peak around 6 A is substantially damped. It should be noticed that the shape and the position of the first peak

change when the density further decreases and the dense vapor region is approached.

3.2 Small angle X-ray scattering

Figure 3 shows selected $S(k)$ of fluid Hg in the M-NM transition, where the density was changed by changing temperature keeping the pressure at 1930 bar. The data are taken from the most recent results [20]. The absolute scale of SAXS intensity for fluid Hg was calibrated using SAXS intensity of compressed He gas. The electronic property of fluid Hg is known to be metallic at the densities from 13.6 to 11.4 g $cm^{-3}$, where we observed no small angle scattering. With decreasing density the electronic transport in fluid Hg changes to a diffusive character in the density region from 11 to 9 g $cm^{-3}$. The $S(k)$ for small $k$ starts to increase around 10 g $cm^{-3}$ and it becomes gradually large with decreasing density. Clear SAXS signals were observed in $S(k)$ around 9.0 g $cm^{-3}$ in the M-NM transition.

When the critical density was approached with further decreasing density, critical opalescence was observed. We analyzed the spectra using the Ornstein-Zernike scattering formula [21], $S(k)= S(0) / (1+\xi^2 k^2)$, where $\xi$ is the correlation length of a density fluctuation and $S(0)$ corresponds to fluctuations in a particle number ($=<(\Delta N)^2/N>$). Figure 4 shows Ornstein-Zernike plots of several $S(k)$ from 0.04 to 0.3 $A^{-1}$ at 1750 bar. The spectra satisfy the scattering law in the wide density region from the fluid at 9.0 g $cm^{-3}$ in the M-NM transition region to the insulating vapor at 4.1 g $cm^{-3}$ through the supercritical region around the critical density of 5.8 g $cm^{-3}$. Data points in the spectra from 9.0 to 8.3 g $cm^{-3}$ are scattered because the SAXS intensity is small.

We carried out least-square fits for the Ornstein-Zernike plots from 0.04 to 0.15 $A^{-1}$ using a linear function and obtained $S(0)$ and $\xi$. The optimized $S(0)$ and $\xi$ are shown as a function of $\rho$ in Fig.5. The values of $S(0)$ and $\xi$ at 1750 bar takes a maximum around 6.2 g $cm^{-3}$ near the critical density of 5.8 g $cm^{-3}$. The peak of $\xi$ is broader than that of $S(0)$. When the critical point is distant with increasing pressure, the maximum values become small and both of the maximum positions shift towards larger $\rho$. The shift with increasing pressure is larger in $\xi$ than $S(0)$. The $S(0)$ values are small in $8 < \rho < 10$ g $cm^{-3}$ compared to the maximum of $S(0)$ around the critical density while the $\xi$ values keep rather large values of about 10 A in the same density region. It should be noticed that the $S(0)$ and $\xi$ values in $8 < \rho < 10$ g $cm^{-3}$ do not change at all with changing pressure. For molecular fluids such as water and $CO_2$, $S(0)$ and $\xi$ increase as the critical point is approached and their maximums are located very close to the critical density and the shapes of $S(0)$ and $\xi$ are very similar [22]. From these facts our data strongly hint that the SAXS intensity without pressure variation observed in $8 < \rho < 10$ g $cm^{-3}$ has an origin different from the critical opalescence.

3.3 Inelastic X-ray scattering

We succeeded in obtaining IXS spectra for expanded fluid Hg in the wide temperature, pressure and density range including the M-NM transition and the liquid-vapor critical regions. Selected IXS data at 13.6 and 9.0 g $cm^{-3}$ are shown in Fig.6 taken from the most recent results [23]. The normalized spectra, $S(k, \omega)/S(k)$, are plotted in the figure, where $\omega$ is the energy transfer. The resolution function is shown by a broken curve at the bottom. The spectra at 13.6

g $cm^{-3}$ have a clear side peak around 10 meV at 0.87 $A^{-1}$. The spectra at 13.6 g $cm^{-3}$ agree well with those reported by Hosokawa et al [24]. The spectra at 9.0 g $cm^{-3}$ have a single peak and the side peaks are not distinct from the central one. Note that the central peaks at 3.71 and 4.68 $A^{-1}$ are much broader at the M-NM transition at 9.0 g $cm^{-3}$ than at 13.6 g $cm^{-3}$. We analyzed the data in the framework of generalized hydrodynamics [25]. The spectra were modeled as the sum of a Lorentzian at zero energy transfer, representing the thermal contribution, and a damped armonic oscillator (DHO) [26] for the sound mode with the statistical occupation factor. We optimized parameters by convolving the model function with the measured resolution function and fitting to the data, as shown in Fig.6. Peaks in the DHO term are well separated at 13.6 g $cm^{-3}$. On the other hand, the DHO term at 9 g $cm^{-3}$ has a heavily damped profile even at the smallest $k$. This behavior suggests a much shorter lifetime of the sound modes at the M-NM transition. Hydrodynamics predicts that viscous liquids exhibit large damping of Brillouin peaks. Similarly, the large damping in the sound mode at 9 g $cm^{-3}$ observed by IXS may be related to the large sound absorption observed in the M-NM transition in fluid Hg using ultrasonic technique [27].

Figure 7 shows the $k$ dependence of the optimized excitation energy $\Omega_Q$ (squares) at 13.6 and 9.0 g $cm^{-3}$ together with sound velocity (dash-dotted lines) obtained by the ultrasonic measurements [28]. Further, dispersion relations (dash-dotted lines) corresponding to 1700 m $s^{-1}$ at 13.6 g $cm^{-3}$ and 1500 m $s^{-1}$ at 9.0 g $cm^{-3}$, respectively, are shown. At 13.6 g $cm^{-3}$, $\Omega_Q$ at large $k$ seems to follow the normalized second frequency moment $\omega_0(k)$ (broken curves), given by $\omega_0(k)^2 = k_B T\, k^2/(mS(k))$, where $k_B$ and $m$ are the Boltzman's constant and a particle mass, respectively. Properly normalized integrals (closed circles) of $S(k,\omega)$ agree with $S(k)$ obtained

from XD [18] (solid curves) at 13.6 g $cm^{-3}$, and $S(k)$ from XD and small-angle X-ray scattering at 9 g $cm^{-3}$, as indicated in the upper panels of Fig.7.

As seen in Fig.7, at 13.6 g $cm^{-3}$ $\Omega_Q$ in the small $k$ region disperses faster than expected from the adiabatic sound velocity and agrees with the dotted line of 1700 m $s^{-1}$. The amount of deviation is about 17 %, in good agreement with previous work [24]. At 9.0 g $cm^{-3}$, the positive deviation is much more pronounced and the effective sound velocity, $v_s(k) = \Omega_Q/k$, is estimated to be 1500 ± 200 m $s^{-1}$, which is triple faster than the ultrasonic sound velocity [28]. When the width of the excitation peak is large, $\Omega_Q$ becomes higher than the peak energy in $S(k,\omega)/S(k)$ but almost corresponds to the peak energy in the current-current correlation function $\omega^2 S(k,\omega)/S(k)$. We confirmed it by plotting the deconvoluted $\omega^2 S(k,\omega)/S(k)$ as shown in Fig.6 (c). We plot the effective sound velocity estimated at 0.2 - 0.43 $A^{-1}$ as a function of $\rho$ in Fig.8 together with the ultrasonic sound velocity [28]. In the metallic region, the positive deviation becomes large with volume expansion and has a strong maximum at the M-NM transition. With further volume expansion to the insulating state, the deviation becomes small. Thus, the large positive dispersion, or fast sound, is observed only in a close vicinity of the M-NM transition. Note that we address the large positive dispersion observed in the present study as 'fast sound', but it may not be the same as the sound speed in high frequency limit defined by the viscoelastic theory on liquid dynamics.

## 4. Discussion

Figure 9 shows the density variation of the coordination number $N$ and the maximum position of $g(r)$, $r_1$, which gives the nearest-neighbor distance. To obtain $N$ from $g(r)$ for fluid

Hg we employed two methods of integration as shown in the figure. In method A, the area up to $r_1$ of $4\pi r^2 n_0 g(r)$ was integrated and doubled, where $n_0$ denotes the average number density of fluid Hg. In method B, the area was integrated up to the first minimum position of $g(r)$, $r_{min}$.

The coordination numbers $N_A$ and $N_B$ obtained by methods A and B, respectively, are plotted in Fig. 9. It should be noted that $N_A$ gives the coordination number in the nearest region of the first neighbor, and $N_B$ is that when the region of the first neighbor is taken as widely as possible. As seen in the figure, $N_B$ decreases substantially and linearly with decreasing density in the wide region from liquid to dense vapor. On the other hand, $N_A$ decreases almost linearly with decreasing density in the metallic region but when the M-NM transition region is approached, around 9-10 g $cm^{-3}$, a deviation from the linear dependence appears. It should be noted that the density around which the deviation starts to occur coincides with the region where the M-NM transition starts to occur. On the contrary, no anomalous behavior is observed in that of $N_B$ around this density region. In the region near the critical density, the variation of $N_A$ changes again. As seen in the figure, $r_1$ in the metallic region remains almost constant. but when the M-NM transition region is approached, $r_1$ starts to slightly increase. Such a behavior coincides with the deviation from the linear dependence of $N_A$. In the region near the critical density, $r_1$ becomes about 3.3 A. From these results we can conclude that the density decrease of fluid Hg is essentially caused by the reduction of the coordination number through the whole density region as seen in the behavior of $N_B$. The variation of $N_A$ and $r_1$ show that three different regions exist in the density. The first one is the metallic region from 13.6 g $cm^{-3}$ to the M-NM transition region where $r_1$ is constant and the coordination number at smaller distance decreases linearly. The second one is the region from 9 g $cm^{-3}$ to the critical density and the third one is

the dense vapor region.

To see the volume dependence of the local structure in liquid Hg more clearly, we tried to reproduce $4\pi r^2 n_0 g(r)$ of fluid Hg from the liquid to the M-NM transition region using a summation of Gaussian peaks. Kaplow et al. [29] pointed out that the local structure of liquid Hg is similar to that of crystalline α-Hg with rhombohedral form. The crystal has an atomic configuration of distorted structure, where six neighboring atoms are hexagonally arranged at 3.5 A around a central atom and other six atoms are located in upper and lower planes three by three. As shown in Fig.10 the asymmetrical first peak of $g(r)$ for liquid Hg at 13.6 g $cm^{-3}$ is well reproduced using two Gaussian peaks, whose positions are 3.0 and 3.6 A, respectively. Their coordination numbers are 6 and 5, respectively. These results appear to be consistent with those reported by Kaplow et al. [29] and may suggest that the local structure of a liquid near the melting point is related that of the crystal below the melting point. Comparing the result at 13.6 g $cm^{-3}$ with that at 9.1 g $cm^{-3}$ in Fig.10, it is evident that the number of atoms coordinated at 3.0 A substantially decreases with decreasing density, while the decrease of the number at 3.6 A is small. These results suggest that during the first stage of volume expansion, Hg atoms are not randomly taken away one by one from the atomic position but especially from closer neighbors. Also, the result suggests that the decrease of atoms coordinated at 3.0 $A^{-1}$ is closely related to the M-NM transition in fluid Hg.

The Reverse Mote Carlo modeling technique was applied to the X-ray diffraction data of expanded fluid Hg using in-house X-ray source [5] by Nield and Verronen [30] and Arai and McGreevy [31]. Their analysis pointed out that the variation of the near neighbors at shorter and longer distance in the first coordination shell is important to understand the nature of the

M-NM transition. The suggestion by these studies is consistent with the results of the Gaussian fitting.

To understand the nature of the M-NM transition in connection with the structural changes of fluid Hg, several band structure calculations were carried out for the hypothetical forms of crystalline Hg. One of the approaches whose principle was consistent with the present experimental results was that of Mattheis and Warren [32]. They assumed that the nearest-neighbor distance was constant, so the density variation in expanded fluid Hg was due entirely to the changes in the coordination number for crystalline Hg with fcc, bcc, sc and diamond structures. They found that the trend of the density dependence of the theoretically calculated density of states is in good agreement with that of the Knight shift in the density range down to about 9.5 g $cm^{-3}$. However, it was found to be necessary to increase the lattice constant to fully open a gap between 6s and 6p bands.

For the understanding of the M-NM transition in expanded fluid Hg taking places at a rather large density of 9 g $cm^{-3}$, it was pointed out that the density fluctuations near the critical point play an important role [33, 34]. By taking fluctuations in the local coordination number into account, Franz [35] showed that a band gap opens at the correct density of 9 g $cm^{-3}$. The model was based on the assumption that the average coordination number decreases linearly with decreasing density, but that the actual local coordination numbers would be randomly distributed over a range. Franz postulated that when a metallic site coordinated by many atoms loses neighboring atoms decreasing the coordination number less than 4, the site is transformed to be insulating and the effect may be propagated over the medium range. When the coordination number substantially decreases, Hg atoms are considered to move around more

easily in the short distance like a free particle which eventually causes the fluctuation of the coordination number. According to the idea of Franz there may appear medium-range fluctuation between the metallic and insulating region.

As mentioned in the section 3.2 the SAXS intensity without pressure variation observed in $8 < \rho < 10$ g cm$^{-3}$ has an origin different from the critical opalescence and might be correlated with such fluctuations intrinsic to the M-NM transition. The $\rho$ dependence of $S(0)$ and $\xi$ in Fig.5, which seems different from that for molecular fluids, may indicate that both of the critical scattering and the weak scattering related to the M-NM transition are overlapped. Then the shift of the peak position with increasing pressure may be due to that the critical scattering intensity decreases while the scattering related to the M-NM transition does not change. The characteristic feature of the density fluctuation in the M-NM transition is that $S(0)$ is small and $\xi$ maintains a large value of about 10 A. The insets of (b) and (c) in Fig.3 show the Ornstein-Zernike and Guinier plots, respectively, at a density of 9.5 g cm$^{-3}$. The statistics are not very good for both plots, but the optimized gyration radius, $R_g$, estimated from the Guinier plot was almost the same value of 10 A as the optimized $\xi$. Thus, there exists an inhomogeneous regime on the scale of about 10 A accompanying the M-NM transition.

To investigate how the density fluctuates accompanying the M-NM transition, we deduced the average number $N$ in a cube with a volume of $\xi^3$ and the fluctuation of particle number $\Delta N$ from $\xi$ and $S(0)$ values. Figure 11 shows the upper and lower limits of local density in the cube, $\rho^+$ and $\rho^-$, as a function $\rho$ at 1930 bar, where $\rho^+$ and $\rho^-$ are defined as $\rho(N+\Delta N)/N$ and $\rho(N-\Delta N)/N$, respectively. The broken line denotes the average density. As seen in the

figure, the $\rho$ dependence of $\rho^+$ and $\rho^-$ clearly changes near 9 g cm$^{-3}$ where the M-NM transition occurs. In the metallic region ($\rho$ > 9 g cm$^{-3}$), $\rho^+$ and $\rho^-$ deviate larger with decreasing $\rho$ and the value of $\rho^+$ is about 13 g cm$^{-3}$ as large as that of liquid Hg at ambient condition. The maximum of the deviation is achieved around 9 g cm$^{-3}$ and then the $\rho^+$ starts to decrease with further volume expansion into insulating state. These facts mean that at the M-NM transition there appears a mixture of metallic and insulating regions. It is also noted that the value of $\rho^+$ around the critical density of 5.8 g cm$^{-3}$ is about 9 g cm$^{-3}$ or less. Kresse and Hafner [36] pointed out by their first principle molecular dynamics simulation that 6s and 6p bands open at 9 g cm$^{-3}$, so the dense region of $\rho^+$ around 5.8 g cm$^{-3}$ may be insulating. Therefore, the critical density fluctuation of fluid Hg is considered to be the fluctuation between insulating liquid and dense vapor. In that sense, the critical fluctuation of fluid Hg may be similar to that of fluid Ar.

It is interesting to discuss the relationship between the medium-range fluctuations and the fast sound accompanying the M-NM transition observed by SAXS and IXS measurements, respectively. Here we do not regard fast sound in the M-NM transition as the high-frequency sound speed in the viscoelastic model. The adiabatic compressibility, $\chi_s$, is related to the sound velocity by $\chi_s = (\rho v_s^2)^{-1}$. Therefore, the fast sound velocity suggests that the microscopic $\chi_s$ is much smaller than the macroscopic one, which means that the mean square fluctuations of microscopic pressure, $\langle(\Delta p)^2\rangle \propto \chi_s^{-1}$ are very large. The enhancement of microscopic $\langle(\Delta p)^2\rangle$ can be caused by a local deformation of a pair potential, $\varphi(r)$, especially its repulsive part, as shown by the pressure equation, $p = n_0 k_B T - (n_0^2/6)\int(\partial\varphi/\partial r)g(r)d\vec{r}$. We consider that such

deformation in a pair potential becomes pronounced at the M-NM transition, due to the fluctuations of local electronic states between metallic and insulating ones suggested by SAXS results. A sign of fluctuations at the M-NM transition is also found in the IXS data as a narrowing of $S(k, \omega)$ at 0.24 $A^{-1}$ at 9.0 g $cm^{-3}$. compared with that at 13.6 g $cm^{-3}$. Thus, the appearance of the fast sound strongly hints that the M-NM transition accompanies intrinsic fluctuations induced by the local deformation of a pair potential. We speculate that pressure fluctuations $<(\Delta p)^2>$ in microscopic space of several 10 A and time of sub-picoseconds where the fast sound waves exist are considered to be averaged and smoothed out as the thermodynamic limit is approached. The SAXS results suggest that such fluctuations after time-averaged have the scale of 10 A and that they are alive as weak $<(\Delta N)^2>$ in the M-NM transition.

Finally we comment on the relation between the present results and macroscopic quantities of fluid Hg in the M-NM transition. Levin and Schmutzler [37] measured the specific heat at constant pressure $C_P$ for expanded fluid Hg from 12.4 to 8.8 g $cm^{-3}$ and deduced $C_V$ using $pVT$-data and a thermodynamic relation. The specific heat ratio $\gamma$ calculated from their data was 1.2 at 12.4 g $cm^{-3}$ and 3.6 at 9.0 g $cm^{-3}$. Similarly, using sound velocity, $pVT$ data and the relation, $\gamma=\chi_T/\chi_s$, where $\chi_T$ is the isothermal compressibility, results consistent with those by Levin and Schmutzler were reported [38, 39]. Thus the large $\gamma$ appears to represent macroscopic anomalies in the M-NM transition in fluid Hg. On the contrary, generalized hydrodynamics predicts that $\gamma$ approaches unity at $k$ infinity limit [25]. Following this prediction, we speculate that information obtained from IXS represents exactly the microscopic

nature in the M-NM transition, both small volumes and high frequencies, in fluid Hg. IXS spectra at large $k$ which approximately exhibit a Gaussian profile at 9 g $cm^{-3}$ suggests that a free particle motion is dominant over short (less than interatomic) distances in the M-NM transition. This result supports the idea that Hg atoms move freely in the interatomic distance causing the fluctuation of the coordination number after the substantial reduction of the coordination number around the M-NM transition region.

## 5. Conclusion

We have measured the static and dynamic structure factors of expanded fluid Hg focusing on the M-NM transition. When liquid Hg expands the coordination number substantially decreases without changing the interatomic distance. When the coordination number decreases down to 4 or 3 a structural instability takes place inducing the fluctuation of coordination number and eventually producing the density fluctuation in the mesoscopic scale between metallic and insulating region. Such a structural instability is a driving force of the M-NM transition in expanded fluid Hg. The fast sound was observed as a result of the fluctuation in the microscopic space and time accompanying the M-NM transition. It was also suggested that the fluctuation inducing the M-NM transition is independent from the critical fluctuation.

## Acknowledgements

The authors would like to thank Professor K. Hoshino and Professor F. Shimojo for the valuable discussions. Dr. K. Funakoshi, Dr. W. Utsumi, Dr. Y. Ohishi, Dr. S. Tsutsui and Dr. A.Q.R. Baron are acknowledged for their collaborations. The authors are also grateful to Dr. X.

Hong, Dr. Y. Sakaguchi, Dr. M.H. Kazi, Mr. H. Itoh, Mr. Y. Itoh, Ms. M. Kusakari, Mr. K. Satoh, Mr. K. Mifune, Mr. Y. Naito, Mr. T. Nishii, Mr. A. Sobajima and Mr. M. Muranaka for their valuable support on the experiments. This work was supported by the Grant-in-Aid for Specially Promoted Research from the Ministry of Education, Science and Culture of Japan under Contact No.11102004 (from April, 1999 to March, 2004). The synchrotron radiation experiments were performed at SPring-8 with the approval of the Japan Synchrotron Radiation Research Institute (The long term proposal from 2000B to 2003A).

References

[1] F. Hensel and E. U. Franck, Ber. Bunsenges. Phys. Chem., **70** (1966) 1154.

[2] W. Freyland, Comment. Solid state Phys., **10** (1981) 1; F. Hensel, M. Stoltz, G. Hohl, R. Winter and W. Goetzlaff, J. Physique, **C5 Suppl-1** (1991) 191.

[3] F. Hensel and W.W. Warren, Jr., *Fluid Metals* (Princeton University Press, New Jersey, 1999).

[4] W.Goezlaff, G.Shoenherr and F.Hensel, Z. Phys. Chem., NF **156** (1988) 219; W.Goezlaff, Ph.D. Thesis, University of Marburg, 1988.

[5] K. Tamura and S. Hosokawa, Phy. Rev. B., **58** (1998) 9030.

[6] G. Franz, W. Freyland, W. Glaeser, F. Hensel and E. Schneider, J. Physique, **C8**, (1980) 194.

[7] R. Winter, F. Hensel, T. Bodensteiner and W. Glaeser, Ber. Bunsenges. Phys. Chem., **91** (1987) 1327.

[8] W. C. Pilgrim, M. Ross, L. H. Yang and F. Hensel, Phys. Rev. Lett., **78** (1997) 3685.

[9] F. Hensel, E. Marcesa and W. C. Pilgrim, J. Phys.:Condens. Matter, **10** (1998) 11395.

[10] S. T. Weir, A. C. Mitchell and W. J. Nellis, Phys. Rev. Lett., **76** (1996) 1860.

[11] K. Tamura, M. Inui, K. Funakoshi and W. Utsumi, Nucl. Instrum. Methods Phys. Res., **A467-468** (2001) 1065.

[12] K. Tamura and M. Inui, J. Phys.:Condens Matter, **13** (2001) R337.

[13] M.Isshiki, Y.Oh'ishi, S.Goto, K.Takeshita and T.Ishikawa, Nucl. Instrum. Methods Phys. Res., **A467-468** (2001) 663.

[14] K.Tamura, M.Inui, T.Matsusaka, D.Ishikawa, M.H.Kazi, X.Hong, M.Isshiki and Y.Oh'ishi, J.Non-Cryst. Solids, **312-314** (2002) 269.

[15] A.Q.R.Baron, Y.Tanaka, D.Miwa, D.Ishikawa, T.Mochizuki, K.Takeshita, S.Goto, T.Matsushita and T.Ishikawa, Nucl. Instrm. Meth. **A467-468** (2001) 627.

[16] M.Inui and K.Tamura, Z. Phys. Chem. **217** (2003) 1045.

[17] K.Tamura, M.Inui and S.Hosokawa, Rev. Sci. Instrm. **70** (1999) 144.

[18] M.Inui, X.Hong and K.Tamura, Phys. Rev. B **68** (2003) 094108.

[19] X.Hong, M.Inui, T.Matsusaka, D.Ishikawa, M.H.Kazi and K.Tamura, J.Non-Cryst. Solids, **312-314** (2002) 284.

[20] M. Inui, K. Matsuda, K. Tamura and D. Ishikawa, J. Cryst. Soc. Jpn. **48** (2006) 76 [in Japanese].

[21] H.E. Stanley, *Introduction to phase transition and critical phenomena* (Oxford University Press, 1971).

[22] K.Nishikawa and I.Tanaka, Chem. Phys. Lett., **244** (1995) 149; K.Nishikawa and T.Morita, Chem. Phys. Lett. **316** (2000) 238; T. Morita et al, J. Chem. Phys. **112** (2000) 4203.

[23] D. Ishikawa, M. Inui, K. Matsuda, K. Tamura, S. Tsutsui and A.Q.R. Baron, Phys. Rev. Lett., **93** (2004) 097801.

[24] S.Hosokawa, H.Sinn, F.Hensel, A.Alatas, E.E.Alp, W.-C. Piligrim, J.Non-Cryst. Solids, **312-314** (2002) 163.

[25] J.P. Boon and S. Yip, *Molecular Hydrodynamics* (McGraw-Hill, New York, 1980).

[26] B.Fak and B.Dorner, Institute Laue-Langevin Report 92FA008S (1992).

[27] H. Kohno and Yao, J. Phys.;Condens. Matter, **13** (2001) 10293.

[28] M.Yao, K. Okada, T. Aoki and H. Endo, J. Non-Cryst. Solids, **205-207** (1996) 274; V. Kozhevnikov, D. Arnold, E. Grodzinskii and S. Naurzakov, J.Non-Cryst. Solids, **205-207** (1996) 256.

[29] R. Kaplow, S.L. Strong and B.L. Averbach, Phy. Rev., **138** (1965) A1336.

[30] V. M. Nield and P. T. Verronen, J. Phys.:Condens. Matter, **10** (1998) 8147.

[31] T. Arai and R. L. McGreevy, J. Phys.:Condens. Matter, **10** (1998) 9221.

[32] L. F. Mattheis and W. W. Warren, Jr., Phys. Rev. B, **16** (1977) 624.

[33] M.H. Cohen and J. Jortner, Phys. Rev. A**10** (1974) 978.

[34] M. Ross and F. Hensel, J. Phys.:Condens. Matter, **8** (1996) 1909.

[35] J. R. Franz, Phys. Rev. Lett., **57** (1986) 889.

[36] G. Kresse and J. Hafner, Phys. Rev. B **55** (1997) 7539.

[37] M. Levin and R. Schumutzler, J. Non-Cryst. Solids, **61-62** (1984) 83.

[38] K. Suzuki, M. Inutake, S. Fujiwaka, M. Yao and H. Endo, J. Phys. (France) **41** (1980) C8-66.

[39] M. Yao and H. Endo, J. Phys. Soc. Jpn., **51** (1982) 966.

Figure captions

Fig.1, Structure factor $S(k)$ for expanded fluid Hg. Temperature, pressure and density are indicated at the upper-side of each curve. The curves are displaced by 1 for clarity. $\rho_C$ and M-NM denote the data near the critical density and M-NM transition, respectively.

Fig.2. Pair distribution function $g(r)$ for expanded fluid Hg obtained from Fourier transform of $S(k)$ in Fig.1. The curves are displaced by 1 for clarity.

Fig.3. (a) Selected structure factors $S(k)$ in the M-NM transition region of fluid Hg at densities from 11.4 to 9.1 g $cm^{-3}$ at 1930 bar obtained from SAXS measurements. The spectra are displaced by 1 for clarity. (b) Ornstein-Zernike and (c) Guinier plots of $S(k)$ at 9.5 g $cm^{-3}$. are shown for comparison.

Fig.4. Ornstein-Zernike plots of selected $S(k)$ for expanded fluid Hg at 1750 bar. The spectra are displaced by 0.5 for clarity.

Fig.5. Plots of $S(0)$ and $\xi$ as a function of $\rho$ at 1750 bar (open circles), 1800 bar (open squares) and 1930 bar (open triangles).

Fig.6. $S(k,\omega)/S(k)$ at several $k$ of fluid Hg at densities of (a) 13.6 and (b) 9.0 g $cm^{-3}$ obtained

from IXS (open circles). Fits (bold solid lines on the data) were made by convolving the resolution function to a model function (dash-dotted curves) combined by Lorenzian (thin broken curves) and DHO peaks (thin solid curves). An example of the resolution function is indicated at the bottom. (c) $\omega^2 S(k,\omega)/S(k)$ calculated using the deconvoluted model function at 9 g cm$^{-3}$.

Fig.7. Upper panels: Open circles denote integrals of IXS data with respect to $\omega$ at (a) 13.6 and (b) 9 g cm$^{-3}$, which are normalized by the atomic form factor and polarization factor. A solid curve show $S(k)$ in Fig.1 [18] at each density. Further, $S(k)$ at small $k$ in Fig.3 is plotted at (b) 9 g cm$^{-3}$.

Lower panels: Excitation energy, $\Omega_Q$ (squares), as a function of $k$ at (a) 13.6 and (b) 9.0 g cm$^{-3}$. Dash-dotted lines denote dispersions following ultrasonic sound velocity [28]. Also shown are the normalized second frequency moment, $\omega_0(k)$ (broken curves) and dispersion (dotted lines) corresponding to 1700 m $s^{-1}$ at (a) 13.6 g cm$^{-3}$ and 1500 m $s^{-1}$ at (b) 9.0 g cm$^{-3}$.

Fig.8. Density dependence of sound velocity taken from the data at low $k$. The dashed line denotes the ultrasonic sound velocity evaluated from Refs. [28].

Fig.9. The coordination number $N_A$ (closed squares) and $N_B$ (closed triangles), and the nearest neighbor distance $r_1$ (closed circles) for expanded fluid Hg as a function of density.

Fig.10. Coordination shells in $g(r)$ at (a) 13.6 and (b) 9.1 g cm$^{-3}$ reproduced using a Gaussian

model. g(r) experimentally obtained is denoted by closed circles. The least-square optimization was carried out for the radial distribution function $4\pi n_0 r^2 g(r)$.

Fig. 11 Local density $\rho^+$ and $\rho^-$ at 1930 bar, obtained from *S(0)* and $\xi$ shown in Fig.5, as a function of average density $\rho$.

Figure1

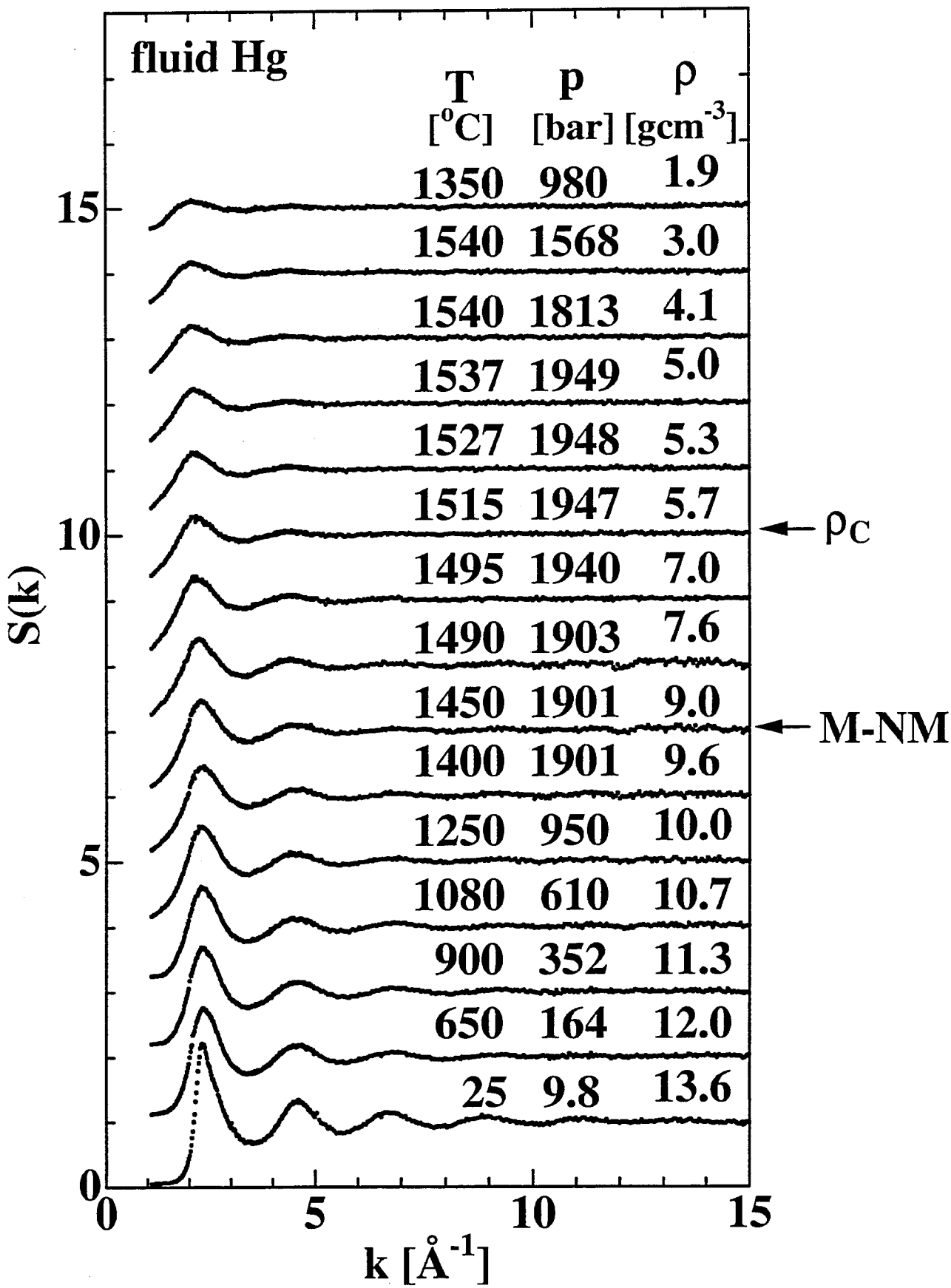
fluid Hg
T [°C]
p [bar]
ρ [gcm-3]
1350 980 1.9
1540 1568 3.0
1540 1813 4.1
1537 1949 5.0
1527 1948 5.3
1515 1947 5.7
1495 1940 7.0
1490 1903 7.6
1450 1901 9.0
1400 1901 9.6
1250 950 10.0
1080 610 10.7
900 352 11.3
650 164 12.0
25 9.8 13.6
ρC
M-NM
S(k)
k [Å-1]
0
5
10
15

Figure2

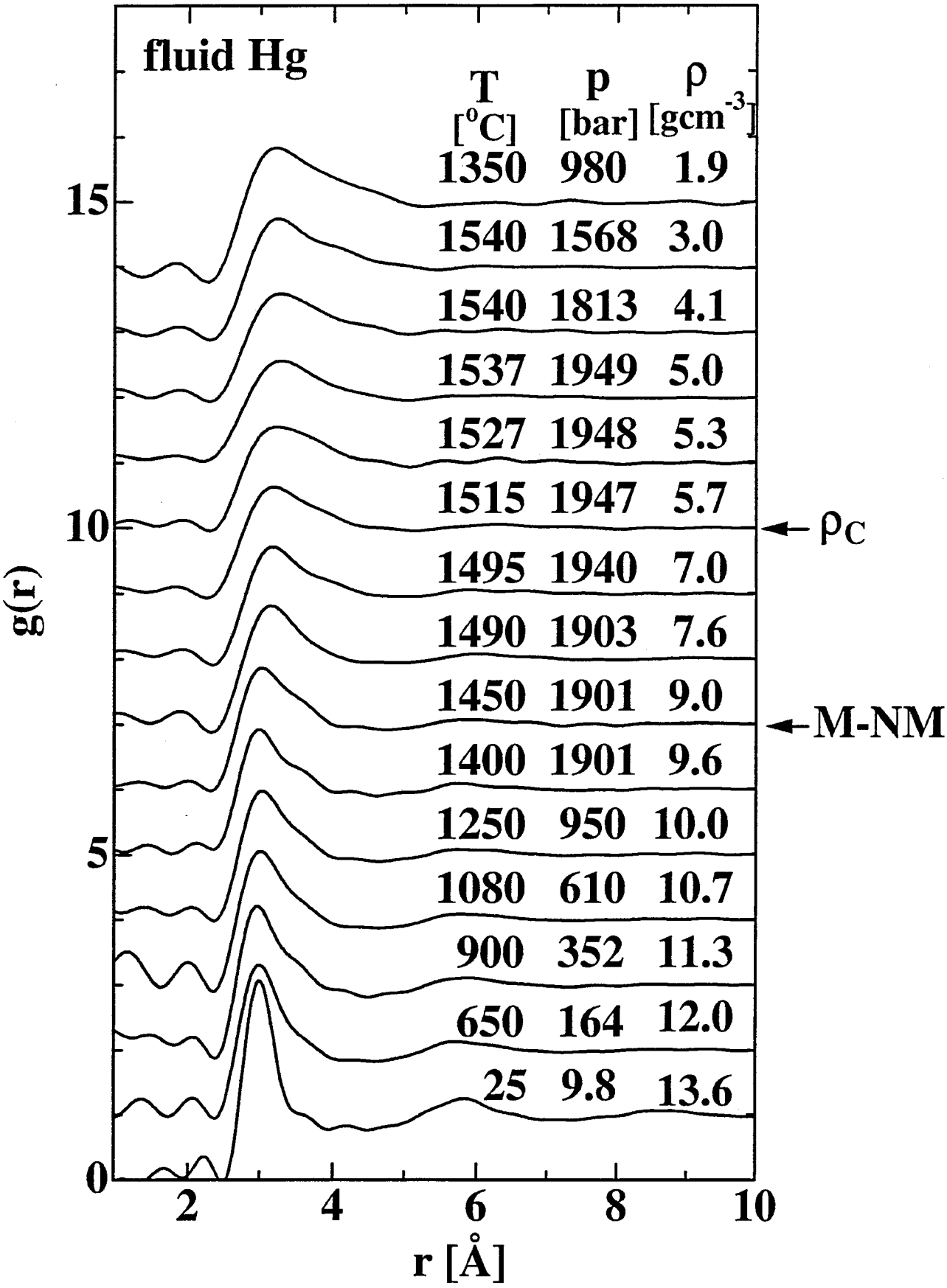
fluid Hg
T [°C]
p [bar]
ρ [gcm-3]
1350 980 1.9
1540 1568 3.0
1540 1813 4.1
1537 1949 5.0
1527 1948 5.3
1515 1947 5.7
1495 1940 7.0
1490 1903 7.6
1450 1901 9.0
1400 1901 9.6
1250 950 10.0
1080 610 10.7
900 352 11.3
650 164 12.0
25 9.8 13.6
ρC
M-NM
g(r)
r [Å]
0
5
10
15
2
4
6
8
10

Figure3

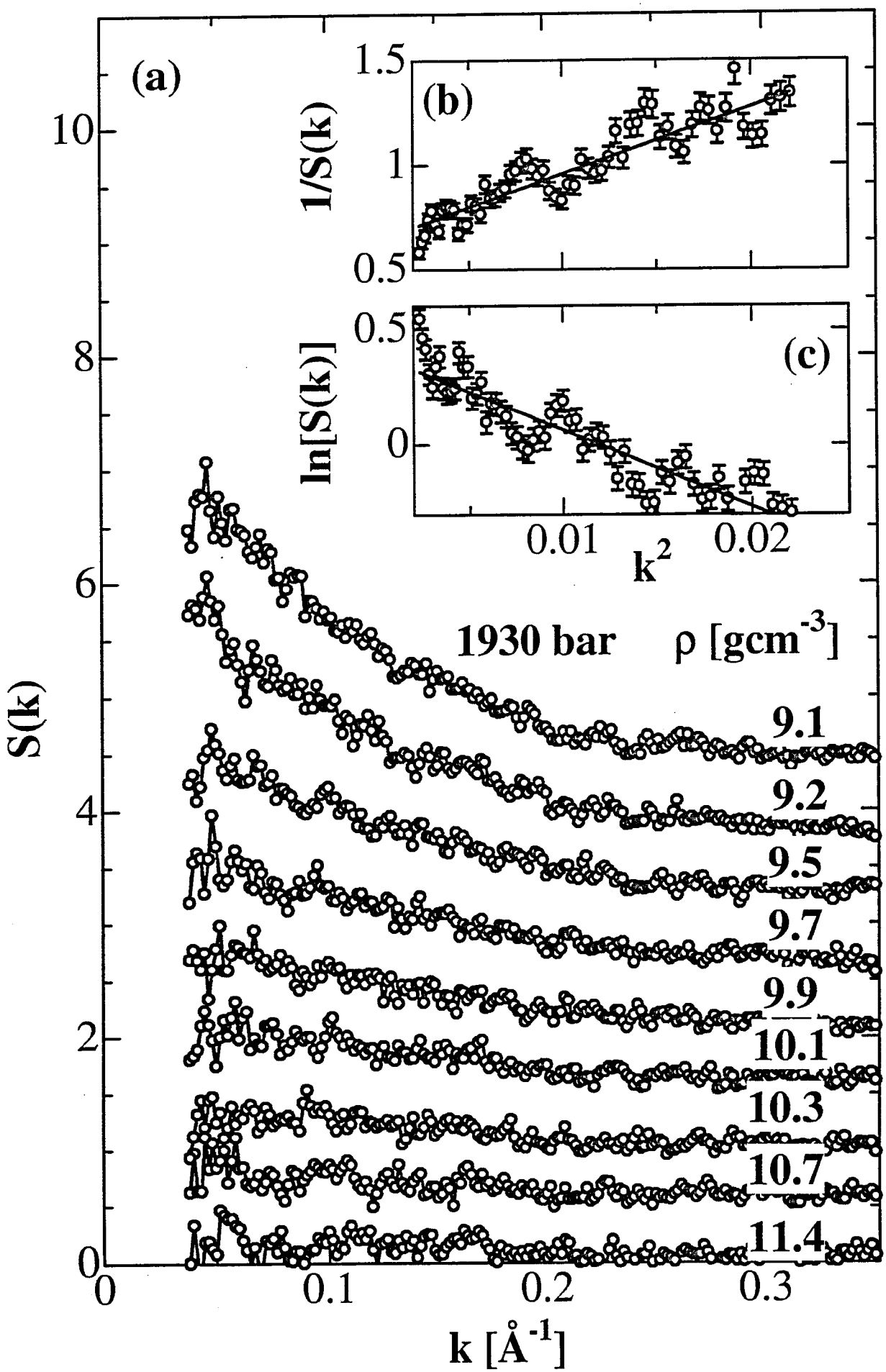
(a)
(b)
(c)
1/S(k)
ln[S(k)]
k²
S(k)
k [Å⁻¹]
1930 bar ρ [gcm⁻³]
9.1
9.2
9.5
9.7
9.9
10.1
10.3
10.7
11.4

Figure4

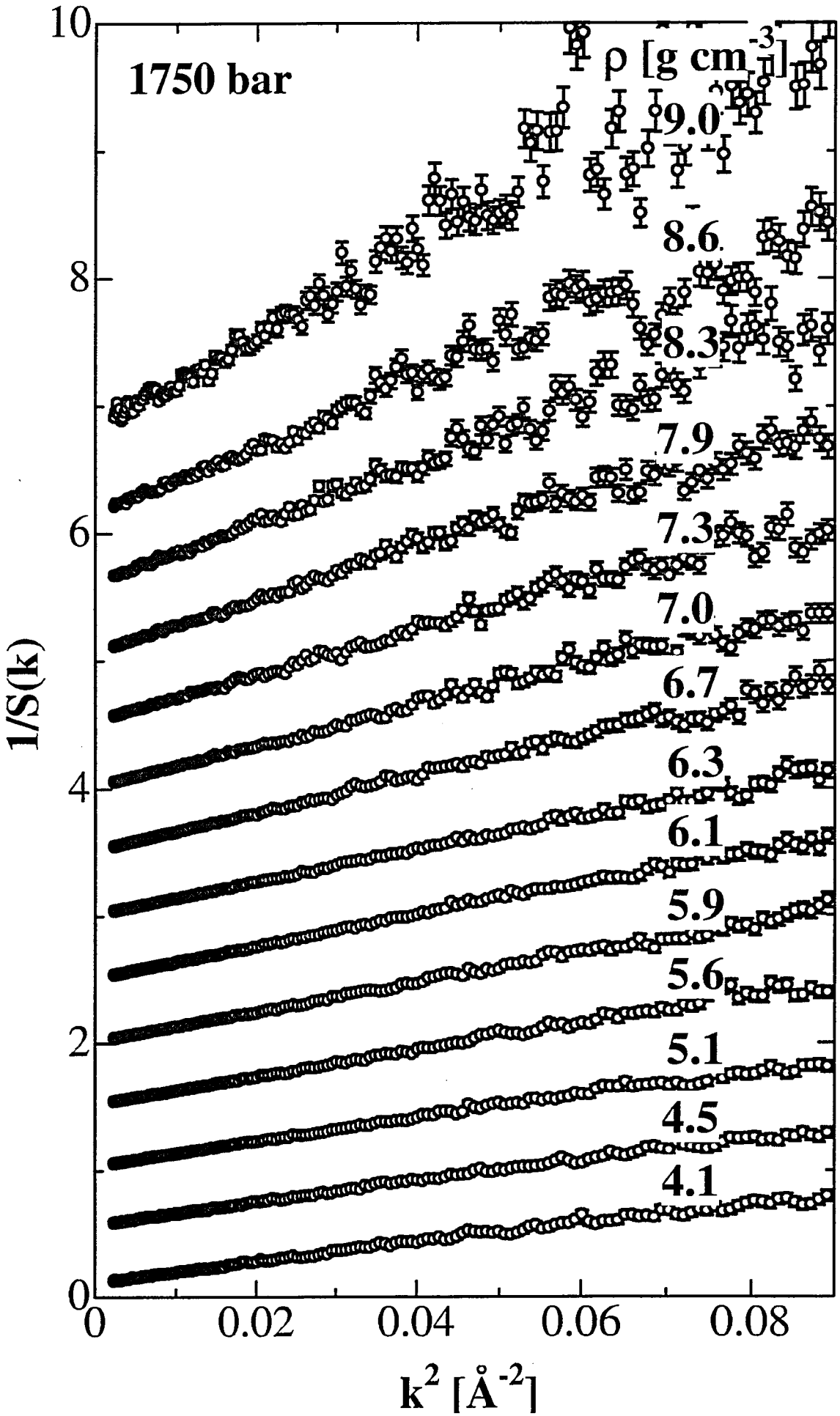
1750 bar
ρ [g cm-3]
9.0
8.6
8.3
7.9
7.3
7.0
6.7
6.3
6.1
5.9
5.6
5.1
4.5
4.1
1/S(k)
k2 [Å-2]
0
2
4
6
8
10
0
0.02
0.04
0.06
0.08

Figure5

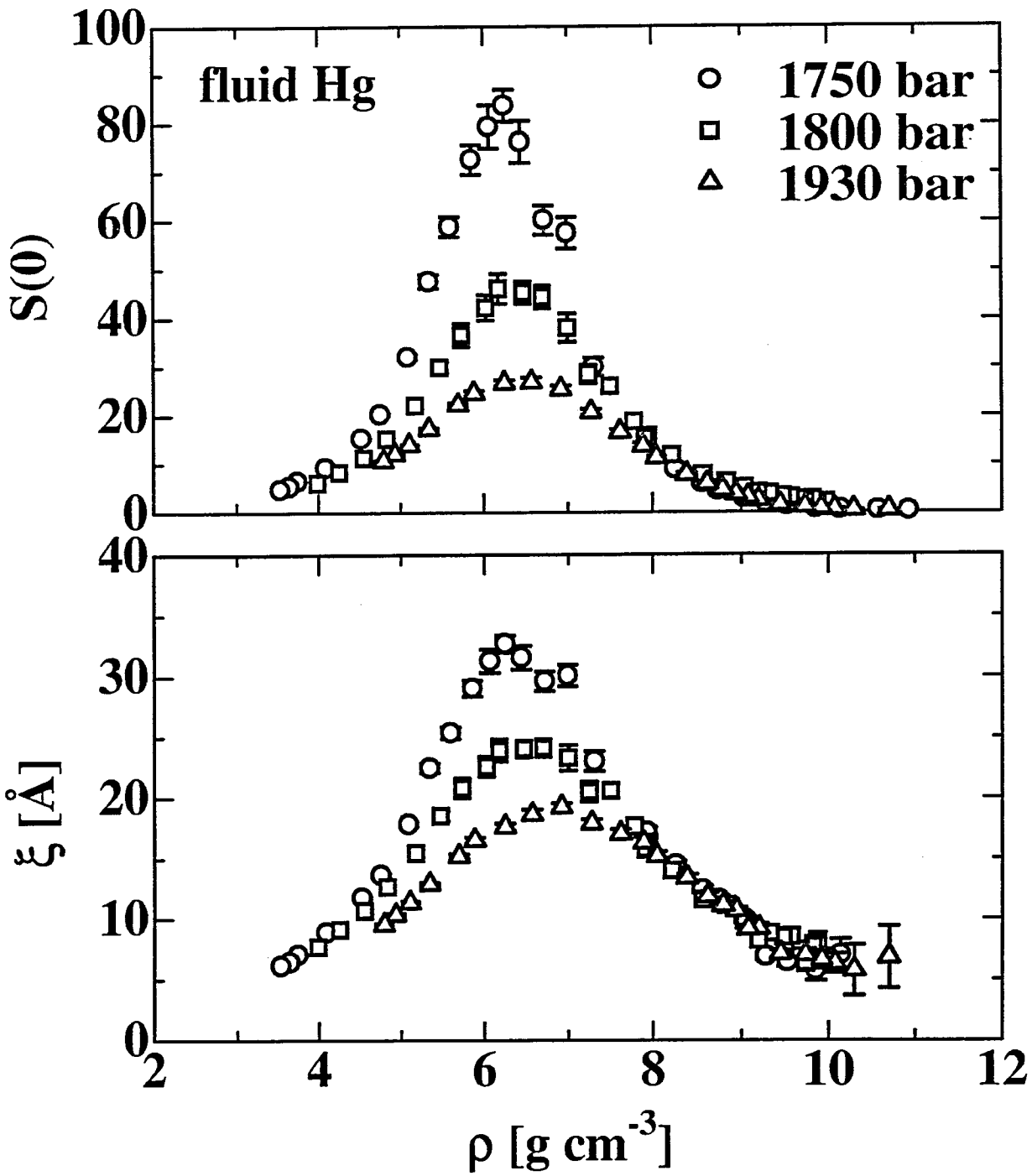
fluid Hg
1750 bar
1800 bar
1930 bar
S(0)
ξ [Å]
ρ [g cm$^{-3}$]
0
20
40
60
80
100
0
10
20
30
40
2
4
6
8
10
12

Figure6

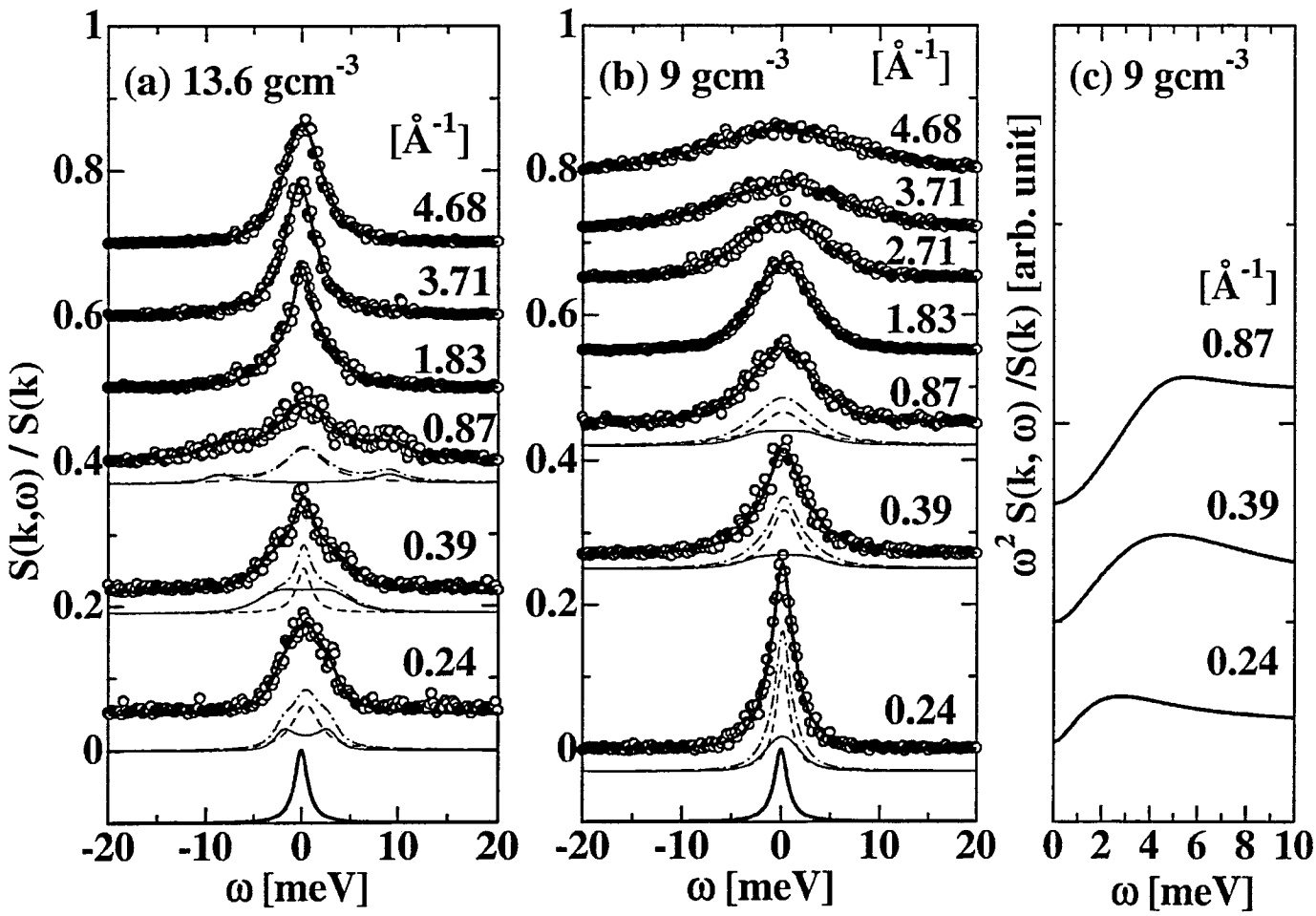
(a) 13.6 gcm-3
[Å-1]
4.68
3.71
1.83
0.87
0.39
0.24
S(k,ω) / S(k)
ω [meV]
(b) 9 gcm-3
[Å-1]
4.68
3.71
2.71
1.83
0.87
0.39
0.24
ω [meV]
(c) 9 gcm-3
[Å-1]
0.87
0.39
0.24
ω2 S(k, ω) /S(k) [arb. unit]
ω [meV]

Figure7

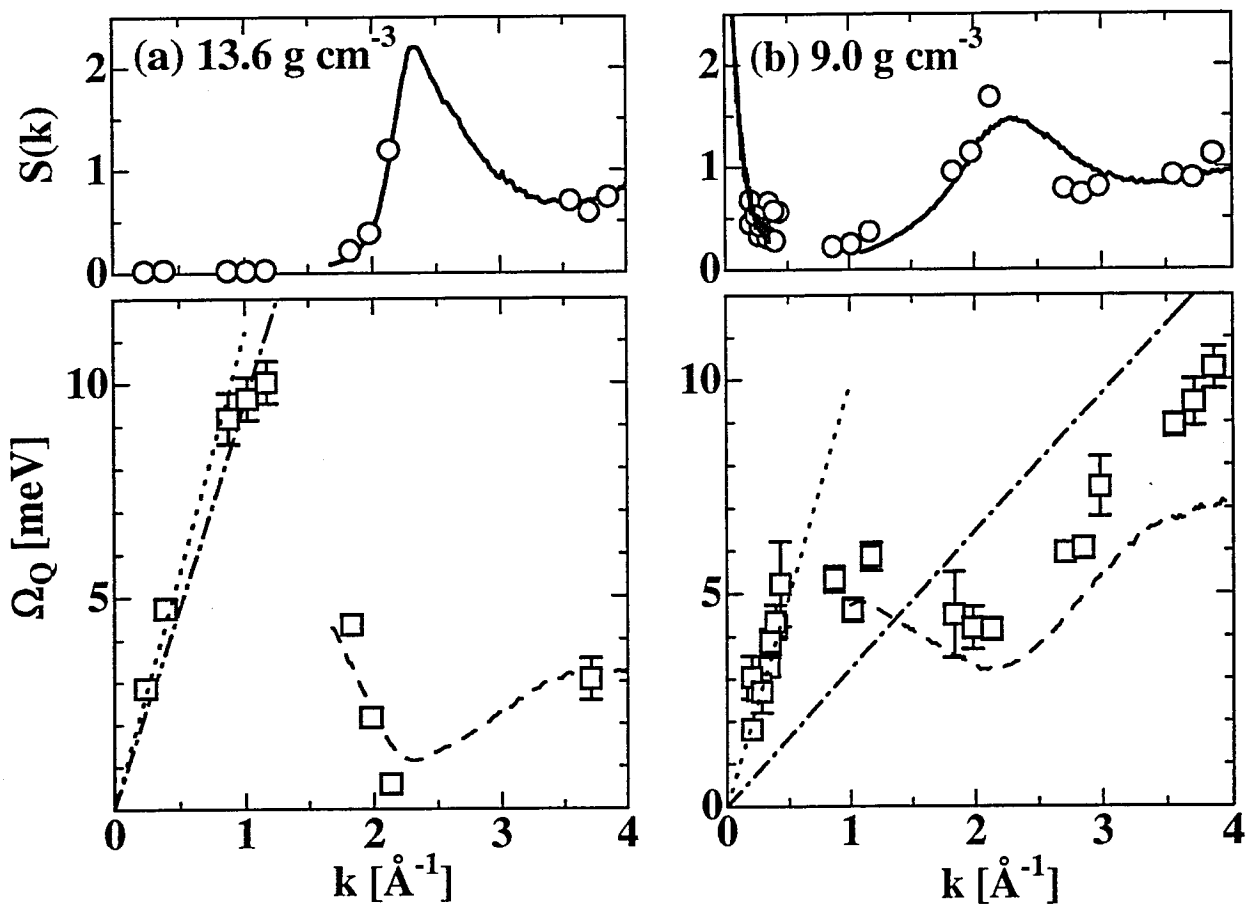

Figure8

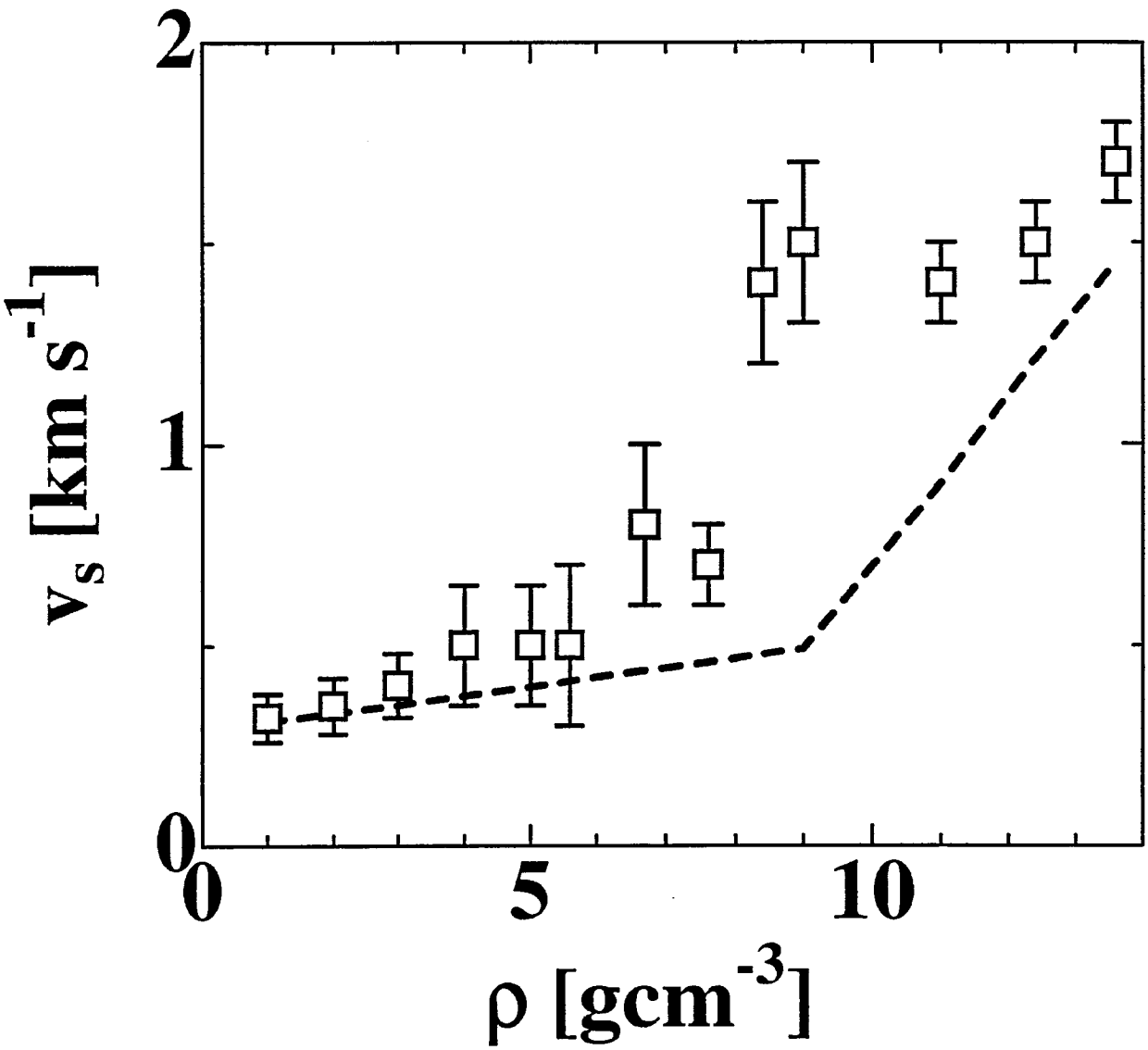

Figure9

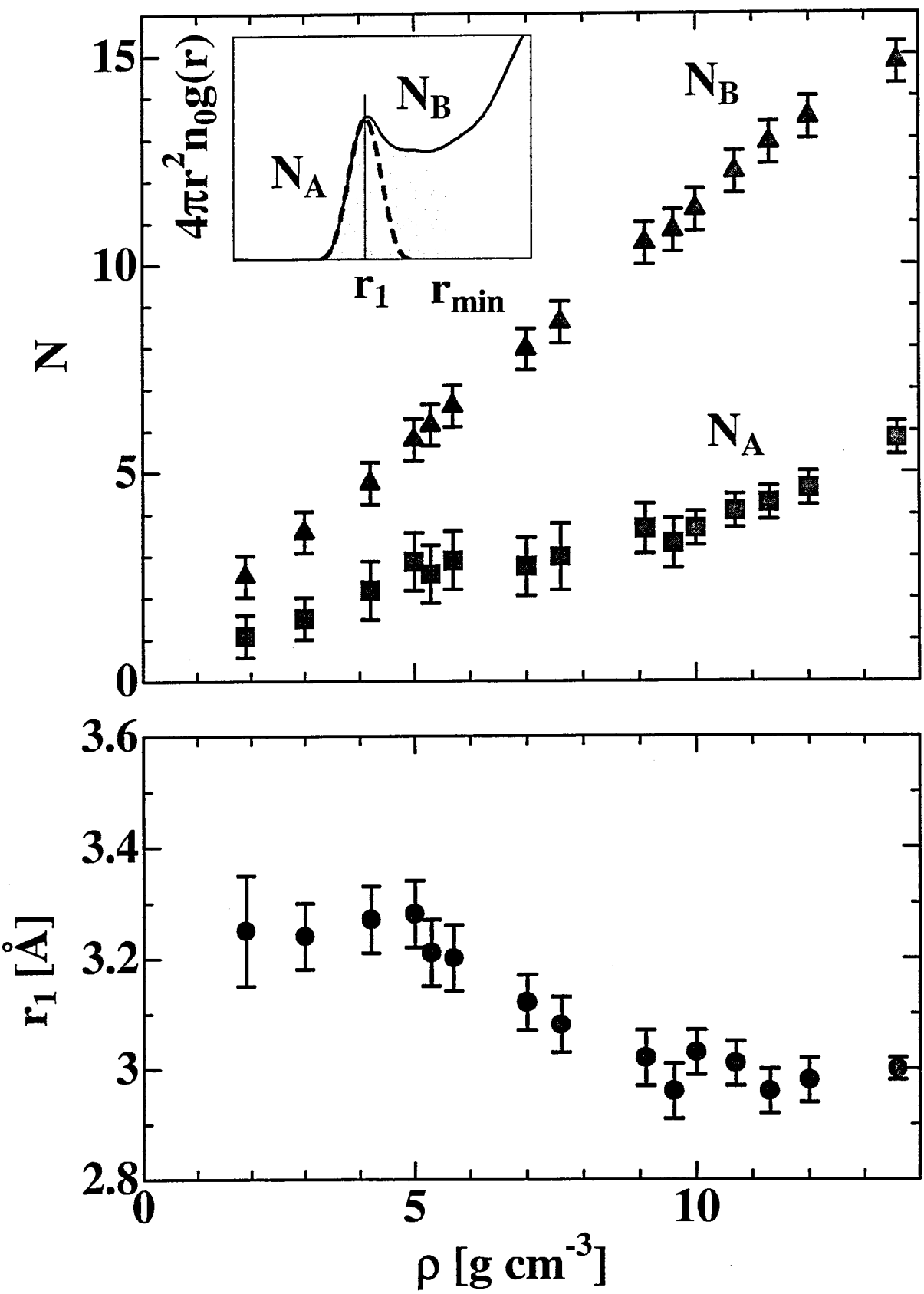
15
10
5
0
N
$4\pi r^2 n_0 g(r)$
$N_A$
$N_B$
$r_1$
$r_{min}$
$N_B$
$N_A$
3.6
3.4
3.2
3
2.8
$r_1$ [Å]
0
5
10
ρ [g cm$^{-3}$]

Figure10

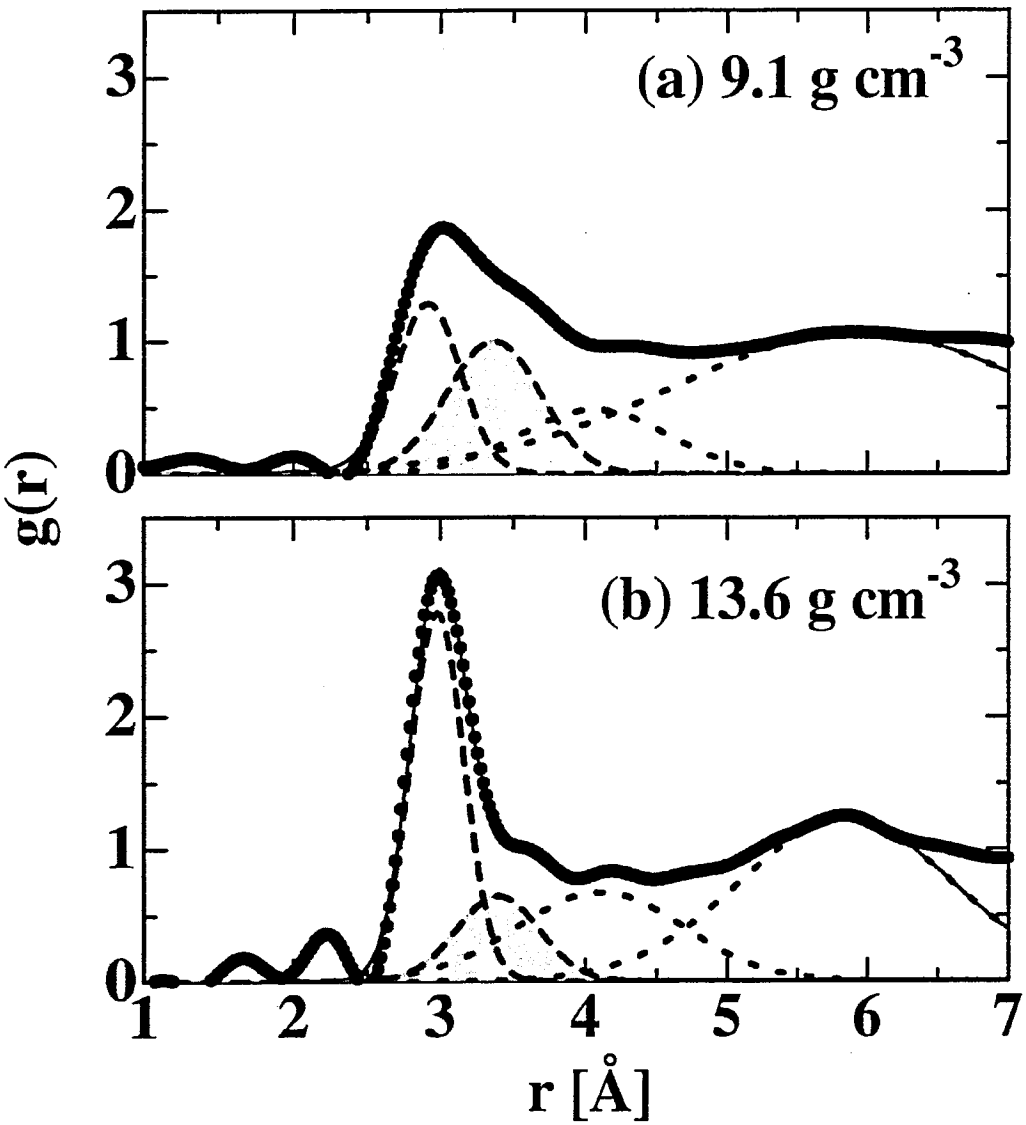

Figure11